TAILORING THERMAL AND CHEMICAL PROPERTIES OF MULTI-FUNCTIONAL THERMAL/ENVIRONMENTAL BARRIER COATINGS

Mackenzie Ridley [a], Hans Olson [b], Kathleen Quiambao-Tomko [b], Patrick Hopkins [b], Elizabeth Opila [a] (Advisor)
[a] University of Virginia, Department of Materials Science and Engineering
[b] University of Virginia, Department of Mechanical and Aerospace Engineering
Virginia Space Grant Consortium
4/9/2021

Abstract: Environmental barrier coatings (EBCs) are required for protection of SiC ceramic matrix composites (CMCs) used in gas-turbine hot sections. Design of multi-functional thermal/environmental barrier coatings (T/EBCs), based on the current state-of-the-art EBC material ytterbium disilicate ($Yb_2Si_2O_7$), was accomplished through multiple rare earth cations mixed in solution. High-temperature high-velocity steam resistance and phase stabilization of multi-component silicate EBCs was observed. Thermal conductivity was decreased up to 70% through increasing bonding and mass heterogeneity in multi-component $RE_2Si_2O_7$, suggesting multi-component rare earth silicates can be tailored as multi-functional T/EBC materials for next-generation turbine components.

Introduction

Ceramic matrix composites (CMCs), introduced into commercial service in 2016 in the GE LEAP engine [1], have a third of the density of traditional superalloys and have a decomposition temperature of 2545 °C, which makes CMCs an ideal alternative to some superalloy components in turbine hot sections [2]. SiC exhibits resistance to high-temperature environments through formation of a protective SiO_2 scale when in contact with oxygen. However, SiO_2 reacts readily with high-temperature water vapor, a byproduct of the gas combustion process, to form a volatile gas species $Si(OH)_4$ (g) [3]. Reaction with water vapor volatilizes the SiO_2, resulting in excessive recession of the structural SiC CMC. Environmental barrier coatings (EBCs) are thus required coatings to mitigate this volatilization. The long-term stability of EBCs in water vapor is currently not well understood.

EBC material design has focused on silicate materials, such as the current state-of-the-art EBC $Yb_2Si_2O_7$, to maintain chemical compatibility with both a required silicon intermediate bond coat and the SiC, to provide greater stability than thermally grown SiO_2, and to provide an acceptable thermal expansion match with the underlying silicon bond coat and SiC CMCs.

It is clear that with increasing fuel burn temperatures of turbines, CMC technology could be limited by the melting temperature of the required silicon bond coat at 1414 °C. One approach to mitigate the melting of silicon is a dual-purpose thermal/environmental barrier coating (T/EBC) system or a multi-layer T/EBC system to decrease operating temperatures of the bond coat while still increasing fuel burn temperatures. A multi-functional T/EBC would primarily require that EBCs have low thermal conductivities to limit heat transport to the bond coat and CMC substrate.

This research focuses on design of next generation T/EBC candidates and tandem study of fundamental EBC reaction mechanisms in high-temperature high-velocity steam. Low thermal conductivities were tailored through multiple rare earth cation solutions in rare earth (RE) disilicates, $RE_2Si_2O_7$. Steam resistance of multi-component $RE_2Si_2O_7$ was determined through high-velocity steam testing at 1400 °C.

Background

The phase diagram for the Yb_2O_3-SiO_2 system is presented in Figure 1, where all other rare earth silicate systems display similar phase stabilities as shown for the Yb-Si-O system. Three line compounds are present on the rare earth silicate phase diagrams: $RE_2Si_2O_7$, $RE_4Si_3O_{12}$ (more recently represented as a RE-deficient $RE_{9.33}\square_{0.67}Si_6O_{26}$ [4,5]), and RE_2SiO_5. The $RE_{9.33}\square_{0.67}Si_6O_{26}$ apatite phase is not well studied in the literature, and is generally only present at temperatures higher than desired EBC use temperatures.

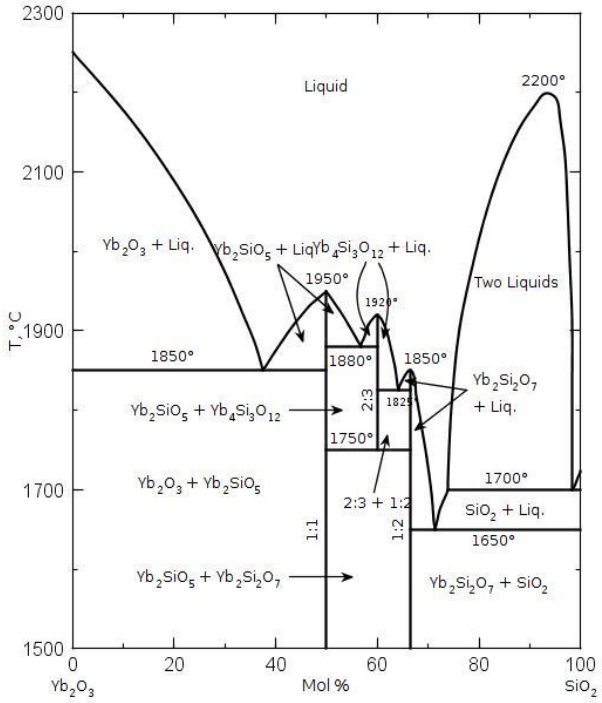

Figure 1. Phase diagram of the Yb_2O_3-SiO_2 system [6], representative of all RE_2O_3-SiO_2 systems.

It has been assumed that all rare earth silicates behave similarly in steam environments through production of a $Si(OH)_4$ (g) species, as shown in Equations (1) and (2).

$$RE_2Si_2O_7 + 2\ H_2O\ (g) \rightarrow RE_2SiO_5 + Si(OH)_4(g) + \text{porosity} \quad (1)$$

$$RE_2SiO_5 + 2\ H_2O\ (g) \rightarrow RE_2O_3 + Si(OH)_4(g) + \text{porosity} \quad (2)$$

Figure 2 shows the seven stable polymorphs for all $RE_2Si_2O_7$, where RE = Sc, Lu, Yb, and Tm do not contain polymorphs and are stable as the β-phase. The β-, γ-, and G-phases are desirable due to their coefficient of thermal expansion (CTE) match with SiC. The stable β-phase is generally desired for EBC material candidates to limit polymorph transitions during thermal cycling. Multi-component rare earth silicates should thus be phase stabilized over the entire temperature range as the β-, γ-, or G- $RE_2Si_2O_7$ phases to prevent phase changes with associated cracking from volume changes during temperature cycling.

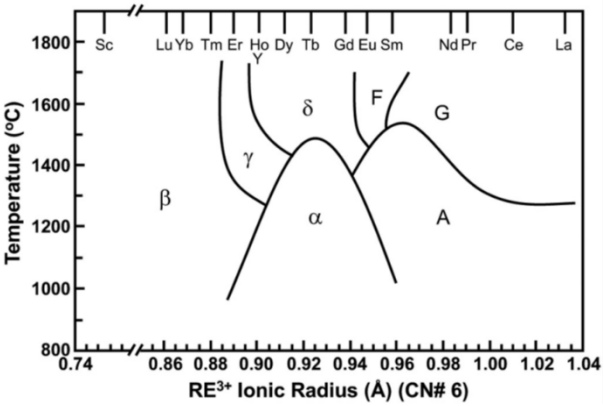

Figure 2. Phase stability of $RE_2Si_2O_7$ relative to rare earth ionic radius [7].

Gas turbine combustion environments contain approximately 10% H_2O (g) as well as unreacted oxygen under high pressures [8], where the high total pressures of gas turbines translates to water vapor partial pressures near 1 atm. Historically, high-temperature water vapor studies have been limited to low total pressures of water vapor or low velocity steam due to complexities in high velocity steam testing setups. The inlet gas velocity for a Model 501-K turbine (Rolls-Royce, Indianapolis, IN) field test at vane mid-span has been measured at ~160 m/s, and the gas stream is further accelerated to ~575 m/s at the vane exit [9]. High velocities are hence vital to steam testing for accurate understanding of thermochemical and thermomechanical stability of EBCs.

The concept of utilizing entropy has revolutionized materials design in many alloy and ceramic systems [10, 11], challenging state-of-the-art materials design. At elevated temperatures, entropy can become a dominating factor for minimizing Gibbs free energy through $\Delta G=\Delta H-T\Delta S$, where ΔG is Gibbs free energy, ΔH is enthalpy, T is temperature, and ΔS is entropy [12]. Minimization of Gibbs free energy can lead to improved material stability at elevated temperatures, where changes in bond strength and melting temperature are hypothesized to contribute to material property changes. A possible example of unique high entropy material properties was noted by Ushakov et al., where a single phase $(La,Sm,Dy,Er,Nd)_2O_3$ solution displayed a measured melting temperature (2456 ± 12 °C) higher than all of the individual constituent oxides [13]. Rare earth silicate specimens containing two or more rare earth cations in solid solution will be referred to as multi-component rare earth silicates in this work.

Research on $(Y_xYb_{1-x})_2Si_2O_7$ showed that the desired beta phase can be stabilized and that the undesired high-temperature polymorphs associated with $Y_2Si_2O_7$ can be avoided, depending on the ytterbium concentration [14]. A high entropy $(Yb_{0.2}Y_{0.2}Lu_{0.2}Sc_{0.2}Gd_{0.2})_2Si_2O_7$ was produced, where the low-CTE β-phase was stabilized for the solid solution [15] despite $Gd_2Si_2O_7$ being stable as the α-phase in the temperature range of interest. A four-component disilicate $(Er_{0.25}Tm_{0.25}Yb_{0.25}Lu_{0.25})_2Si_2O_7$ was processed by Sun et al., where the traditionally stable high-temperature polymorphs for $Y_2Si_2O_7$ and $Tm_2Si_2O_7$ were not present for the solution, further solidifying the concept of phase stabilization for rare earth silicates [16]. Yet, the concept of tailoring phase stability regarding EBC steam resistances and the steam reaction products has not yet been addressed.

Methods

The following multi-component $RE_2Si_2O_7$, were produced, alongside each individual single rare earth (RE) cation $RE_2Si_2O_7$: $(Sc_{0.33}Yb_{0.67})$, (Sc,Y,Yb), (Er,Yb,Lu), (Y,Er,Yb,Lu), $(Sc_{0.15}Y_{0.4}Er_{0.5}Yb_{0.5}Lu_{0.45})$, and (Sc,Nd,Er,Yb,Lu). Equimolar compositions are implied when no subscripts are listed. For brevity in this work, results for equimolar $(Sc,Nd,Er,Yb,Lu)_2Si_2O_7$ will be discussed in detail. Samples were produced from high purity pre-reacted $RE_2Si_2O_7$ powders (Praxair: Danbury, CT). Powders were mixed by ball milling with yttria stabilized zirconia milling media for 24 hours. Powders were then loaded into a 20 mm diameter graphite die and sintered in an argon atmosphere using spark plasma sintering (DCS 25-10 SPS, Thermal Technologies, Santa Rosa, Ca.) at 65 MPa with maximum temperatures of 1550 to 1600 °C for 30 minutes. Resulting pucks were placed in an open-air box furnace (CM Rapid Furnace, Bloomsfield NJ) for 24 hours at 1400 °C to 1500 °C for equilibration. Sample coupons were sectioned from the annealed pucks to produce 10x10x1 mm coupons and polished to 0.25 µm with diamond suspension prior to characterization and steam exposures.

A modified horizontal tube furnace, termed a steamjet [17], was used in this research to model turbine environments. The steamjet simulates a 10 atm turbine environment containing 10% H_2O (g) by maintaining 1 atm steam at the sample impingement site. Deionized water was pumped into a 1 mm diameter Pt-Rh capillary, passing through a 900 °C preheater, and into the tube furnace hot zone held at 1400 °C. The water in the capillary was vaporized in the preheater section, which accelerated steam flow into the tube furnace.

The sample was held in place on an Al_2O_3 holder with platinum wire at a 45-degree angle relative to the capillary outlet. Platinum foil was used between the sample

and Al_2O_3 holder to limit direct contact contamination. The test specimen was placed 1 mm away from the capillary exit in the furnace hot zone, where the proximity of the sample to the capillary outlet allowed for high-velocity steam to impinge upon the sample surfaces with a water vapor partial pressure of 1 atm, thus preventing tube furnace impurities from reacting with the sample regions of interest.

Gas velocities were experimentally controlled through input of the liquid water flow rate (~2 g/min) and experimental setup geometry. ANSYS (Canonsburg, PA) computational fluid dynamics software was used to model the water vapor velocity distribution across the surface of the sample. A maximum velocity of ~240 m/s at 1400 °C was calculated for a 2 ml/min liquid water flow rate, as shown in Figure 3. ANSYS velocity maps were correlated to local depletion depths and microstructural features to a water vapor velocity.

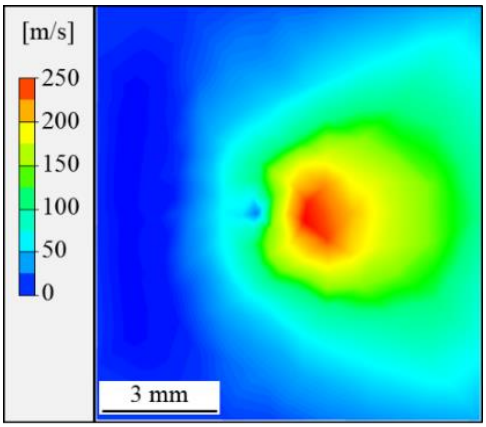

Figure 3. ANSYS Computational Fluid Dynamics Model for steam velocity distribution across the sample face at 1400 °C.

Each $RE_2Si_2O_7$ coupon was exposed to steam at 1400 °C for 125 hours. Sample mass was recorded before and after exposure (MS105DU, Mettler-Toledo, Columbus, OH). X-ray diffraction (XRD, Panalytical Empyrean X-ray diffractometer Westborough, MA) and scanning electron microscopy (SEM: FEI Quanta 650, Hillsboro, OR) with energy dispersive spectroscopy (EDS: Oxford Instruments, Abingdon, UK) were used for analysis in plan view to determine surface reaction products. Coupons were then mounted in cross-section and polished through the center of the highest velocity impingement site for further SEM/EDS analysis to measure SiO_2 depletion depths and morphology changes. Cross-section SEM images were analyzed in ImageJ Analysis Suite (National Institutes of Health, Bethesda, Maryland). SiO_2 depletion depth measurements were taken around 70-110 µm apart across 2-7 mm cross section distances, depending on the region of interest.

Room-temperature thermal conductivity was measured via steady-state thermo-reflectance (SSTR) laser technique [18]. SSTR utilizes a split-beam laser as both a steady-state heat source for the sample and as a subsequent probing laser to discern changes in the sample reflectance, where thermoreflectance was correlated to thermal conductivity through an aluminum thin film transducer deposited on the sample surfaces. Laser measurements of thermal conductivity allowed for measurement of inherent material thermal conductivities, without added effects from impurity phases, grain boundaries, cracks, or porosity. Samples were polished to less than 50 nm average surface roughness prior to aluminum deposition and SSTR measurements.

Results

The starting microstructures of multi-component $RE_2Si_2O_7$ are presented on Figure 4, where all samples except for $(Sc,Nd,Er,Yb,Lu)_2Si_2O_7$ were single phase from SEM/EDS and XRD analysis. $(Sc,Nd,Er,Yb,Lu)_2Si_2O_7$ was found to be multi-phase, consisting of both the β- and G-phases, where Er and Nd cations were concentrated in the G-phase. The G-phase is traditionally a high-temperature polymorph (Figure 2) implying that Er and Nd were phase-stabilized after processing and annealing.

High-velocity Steam Exposures

Figure 5 displays XRD of $(Sc,Nd,Er,Yb,Lu)_2Si_2O_7$ before and after steam exposure. After steam exposure, the sample surface displayed XRD peaks corresponding to the X2-phase RE_2SiO_5, as shown by the Yb_2SiO_5 reference pattern in green.

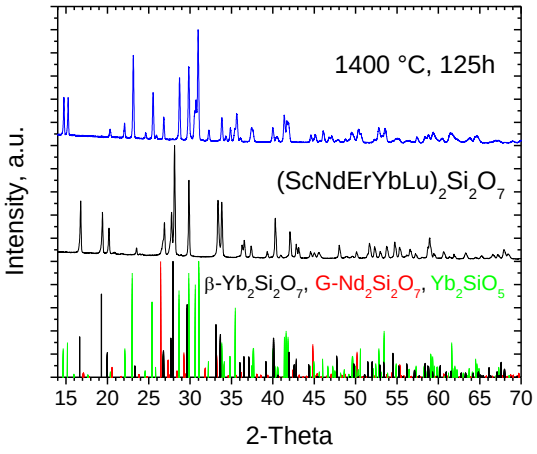

Figure 5. XRD analysis of starting $(Sc,Nd,Er,Yb,Lu)_2Si_2O_7$ (black) and the same sample after steam exposure at 1400 °C and 125 hours, where an X2-phase RE_2SiO_5 solid solution phase was present (blue).

Backscattered electron SEM images of the sample surface are shown in Figure 6. Where local steam velocities were 180-200 m/s, the surface displayed a discontinuous layer of RE_2O_3 on the surface, determined by EDS analysis. At local gas velocities of 100-120 m/s, the initial formation of RE_2O_3 was found on top of RE_2SiO_5. Finally, at local gas velocities of 60-80 m/s, a porous RE_2SiO_5 phase was present on the surface, representative of the primary phase detected by XRD analysis.

EDS mapping of the $(Sc,Nd,Er,Yb,Lu)_2Si_2O_7$ cross-section after steam exposure for 125 hours at 1400 °C is presented in Figure 7 for a region where the local steam velocity was 80-100 m/s. RE_2SiO_5 formation was verified with EDS, as shown by the porous and silicon-depleted product layer on the surface. The initial segregation of Nd and Er cations remained present in the base material after testing, while the steam reaction product was uniquely a single-phase high entropy solid solution, $(Sc,Nd,Er,Yb,Lu)_2SiO_5$. Nd_2SiO_5 is traditionally stable as X1-phase RE_2SiO_5 [19], which implies the high entropy steam reaction product stabilized the Nd cation as the present X2-phase RE_2SiO_5.

Cross-section SEM images of multi-phase $(Sc,Nd,Er,Yb,Lu)_2Si_2O_7$ after steam exposure for 125 hours at 1400 °C are shown in Figure 8, where local steam velocities were: a. 80-120 m/s, b. 150-180 m/s, and c. 200-240 m/s. At gas velocities greater than 130-150 m/s, the $(Sc,Nd,Er,Yb,Lu)_2SiO_5$ product layer displayed sintering and densification which decreased the total reaction depth relative to the intermediate gas velocity range of 80-120 m/s. Material loss and cracking at the highest velocity steam impingement site were due to mechanical erosion for the high velocities. A summary of all measurements for each silicate material is presented on Table 3.

Thermal Conductivity

Room temperature thermal conductivity values measured in this study and in the literature for single and multi-component $RE_2Si_2O_7$ are presented in Table 1 and Table 2. No measurements, calculations, or estimations of thermal conductivity were found for $Nd_2Si_2O_7$ or $Er_2Si_2O_7$. The thermal conductivity of $Lu_2Si_2O_7$ measured in this study (8.7 ± 0.7) was double that of both measurements in the literature (4.4 W/mK [20] and 4.3 W/mK [7]). Presented literature comparisons were performed by laser flash technique, which may include effects of impurity phases, grain boundaries, and porosity distribution.

Table 1. Thermal conductivity, κ, of single cation $RE_2Si_2O_7$ compared to literature values.

$RE_2Si_2O_7$, RE, phase	κ (W/mK), 25 °C, This Study	κ (W/mK), 25 °C, Literature
Sc, β-	9.3 ± 0.5	9.4 [7]

Y, β-	6.3 ± 0.5	5.2 [7], 5.4 [20]
Nd, A-	1.2 ± 0.2	Not available
Er, β-	4.6 ± 0.4	Not available
Yb, β-	5.5 ± 0.5	4.3 [7], 4.45 [20]
Lu, β-	8.7 ± 0.7	4.3 [7], 4.4 [20]

Table 2. Thermal conductivity of multi-component $RE_2Si_2O_7$.

$RE_2Si_2O_7$, RE, phase	κ (W/mK), 25 °C, This Study
$(Sc_{0.33}Yb_{0.67})$, β-	3.0 ± 0.3
(Sc,Y,Yb), β-	2.2 ± 0.3
(Er,Yb,Lu), β-	6.3 ± 0.5
(Y,Er,Yb,Lu), β-	4.3 ± 0.4
$(Sc_{0.15}Y_{0.4}Er_{0.5}Yb_{0.5}Lu_{0.45})$, β-	2.5 ± 0.3

Analysis

High-velocity Steam Exposures

Steam exposure of multi-component $(Sc,Nd,Er,Yb,Lu)_2Si_2O_7$ resulted in primarily a single phase RE_2SiO_5 reaction product with small amounts of a discontinuous RE_2O_3 phase at the highest gas velocities. While the base material was multi-phase, the primary reaction product was single phase within the resolution of EDS and XRD analysis. Both bulk $Sc_2Si_2O_7$ and $Nd_2Si_2O_7$ samples (data not shown in this work) were the only samples which did not form RE_2SiO_5 as the primary steam reaction product. Instead, exclusively Sc_2O_3 and $Nd_{9.33}\square_{0.67}Si_6O_{26}$ phases were present, respectively. The addition of Sc and Nd cations into the disilicate solution did not result in the formation of either excess RE_2O_3 or the apatite phase, suggesting the steam reaction products for multi-component $RE_2Si_2O_7$ can be tailored through cation substitutions.

The sintering of the steam reaction products at gas velocities greater than 130-150 m/s occurred for all $RE_2Si_2O_7$ in this study except for $Sc_2Si_2O_7$, which reacted with steam to exclusively produce Sc_2O_3 as the singular reaction product. This beneficial microstructural change allowed for most materials to display decreased steam reaction depths in the more aggressive environment at the higher gas velocities. The lack of sintering of Sc_2O_3 is presumably due to the high melting temperature of Sc_2O_3 (2472 °C) relative to the RE_2SiO_5 phase (1950-2000 °C).

Multicomponent $RE_2Si_2O_7$ displayed average steam reaction depths comparable to their individual rare earth silicate constituents, as shown in Table 3. Thus, mixing of rare earth cations in solution did not result in large deviations from the average reaction depths of state-of-the-art EBC material, $Yb_2Si_2O_7$. Additionally, the impingement erosion depth was the lowest for the multi-phase $(Sc,Nd,Er,Yb,Lu)_2Si_2O_7$, suggesting multi-phase materials may show increased structural integrity under high velocity steam erosion. Future work should investigate the time, temperature, and velocity dependences for the steam reactions with presented materials to appropriately rank multi-component $RE_2Si_2O_7$ in terms of steam resistance.

Thermal Conductivity

Figure 9 displays the ratio of the measured thermal conductivity divided by the rule of mixtures value on the y-axis, plotted against the standard deviation of the rare earth ionic radius on the x-axes. As the measured thermal conductivity decreases compared to the rule of mixtures, the ratio decreases below a value of one. Thermal conductivity was decreased to ~30% of the predicted rule of mixtures value for $(Sc,Y,Yb)_2Si_2O_7$, which displayed the largest amount of rare earth cation bond heterogeneity. A similar trend was also seen as part of this work for multi-component RE_2SiO_5, presented elsewhere [19].

These results demonstrate that thermal conductivity can be most effectively tailored below the ROM value through further increasing the lattice heterogeneity. This trend has been validated in previous studies where deviations from a ROM thermal conductivity are attributed to phonon scattering from increased lattice disorder [21–23]. In this case,

disorder arises from rare earth cation mass and bonding heterogeneity.

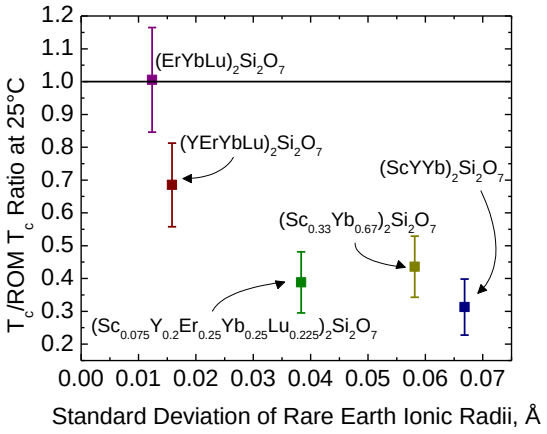

Figure 9. Ratio of measured thermal conductivities divided by the rule of mixtures thermal conductivities on the y-axis for multi-component $RE_2Si_2O_7$, plotted against the standard deviation of rare earth ionic radius on the x-axis.

Conclusion

Multiple rare earth cation solutions were produced to analyze high-velocity steam resistance and to tailor thermal conductivity for multi-functional thermal/environmental barrier coating systems. The steam resistance of multi-phase $(Sc,Nd,Er,Yb,Lu)_2Si_2O_7$ was discussed in detail. The two-phase stabilization of a low CTE G- and β- $RE_2Si_2O_7$ phases was achieved prior to steam testing. Upon steam testing, a solid solution RE_2SiO_5 reaction product phase was present, where Nd_2SiO_5, typically the high CTE X1-phase RE_2SiO_5 [19], was phase stabilized as the low CTE X2-phase RE_2SiO_5. Additionally, the introduction of both Sc and Nd cations did not result in detrimental formation of Sc_2O_3 or Nd silicate apatite reaction products, as was observed with bulk single phase $Sc_2Si_2O_7$ and $Nd_2Si_2O_7$, respectively. The thermal conductivity of multicomponent $RE_2Si_2O_7$ was rapidly decreased through increasing lattice disorder, where rare earth cations of disparate mass and ionic radii were mixed in solution to promote phonon dispersion along the crystal lattice. The results presented here suggest that $RE_2Si_2O_7$ can be tailored with desired low thermal conductivity, and that phase-stabilization of both the bulk EBC material and its steam reaction product can be utilized for controlling the EBC-steam reaction process. Multi-component $RE_2Si_2O_7$ should thus be considered as next-generation T/EBC materials for turbine applications.

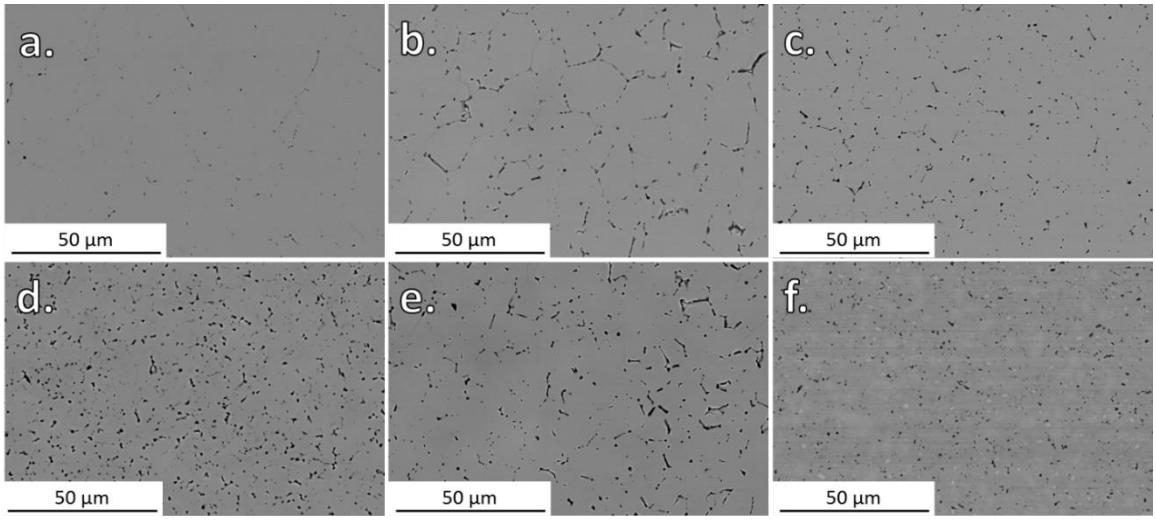

Figure 4. Starting microstructures of multi-component $RE_2Si_2O_7$, for RE = a. $(Sc_{0.33}Yb_{0.67})$, b. (Sc,Y,Yb), c. (Er,Yb,Lu), d. (Y,Er,Yb,Lu), e. $(Sc_{0.15}Y_{0.4}Er_{0.5}Yb_{0.5}Lu_{0.45})$, and f. multi-phase (Sc,Nd,Er,Yb,Lu).

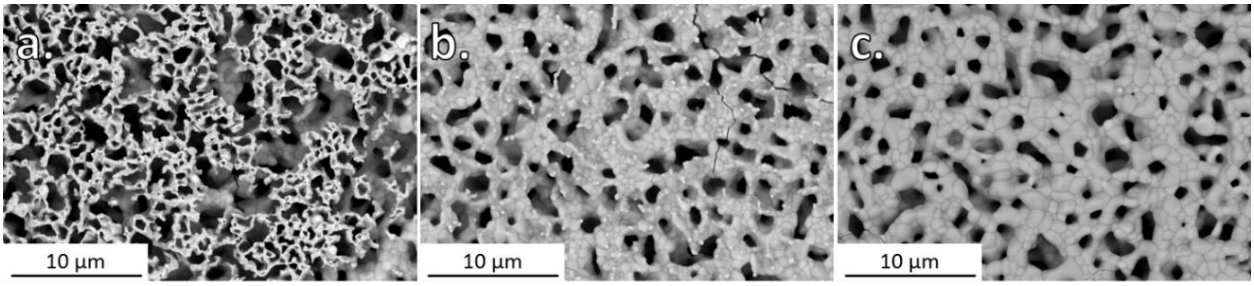

Figure 6. Plan view of $(Sc,Nd,Er,Yb,Lu)_2Si_2O_7$ after steam exposure for 125 hours at 1400 °C, where local steam velocities were: a. 180-200 m/s (discontinuous RE_2O_3 layer on surface), b. 100-120 m/s (Initial RE_2O_3 formation on porous RE_2SiO_5), and c. 60-80 m/s (porous RE_2SiO_5 was present as the primary steam reaction product).

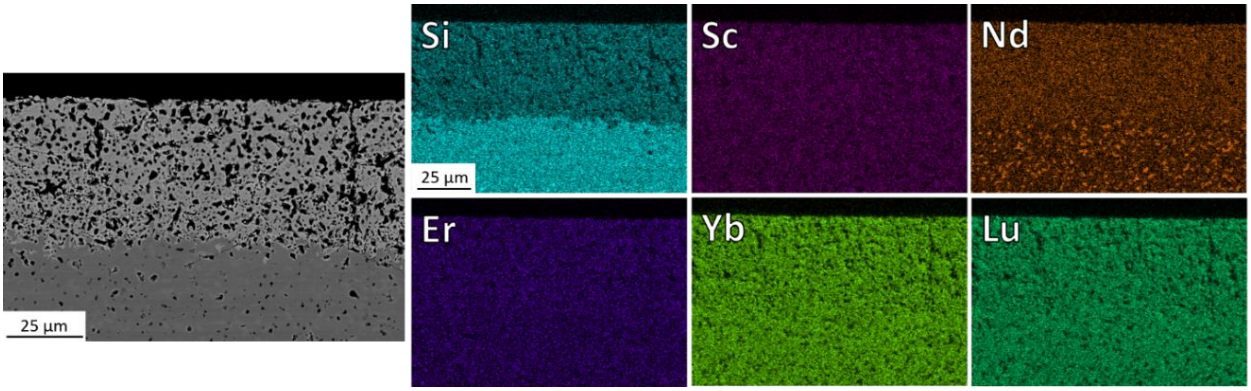

Figure 7. EDS mapping of $(Sc,Nd,Er,Yb,Lu)_2Si_2O_7$ cross-section after steam exposure for 125 hours at 1400 °C and steam velocity 80-100 m/s, where the porous steam reaction product (RE_2SiO_5) formed as a solid solution of all rare earth cations.

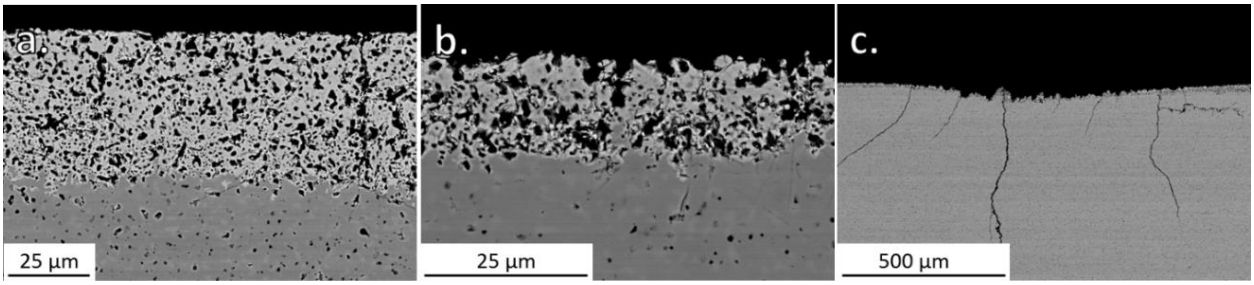

Figure 8. Cross-section SEM images of multi-phase $(Sc,Nd,Er,Yb,Lu)_2Si_2O_7$ after steam exposure for 125 hours at 1400 °C, where local steam velocities were: a. 80-120 m/s, b. 150-180 m/s, and c. steam impingement site, 200-240 m/s.

*Table 3. Specific mass loss and reaction depths for single cation and multi-component $RE_2Si_2O_7$ after steam exposure for 125h at 1400 °C. *$Sc_2Si_2O_7$ reaction depth was averaged over the entire 80-200 m/s steam velocity range for exclusively Sc_2O_3 formation. ⁺$Nd_2Si_2O_7$ reaction depths are presented exclusively for $Nd_{9.33}\square_{0.67}Si_6O_{26}$ formation.*

$RE_2Si_2O_7$, RE	Average Reaction Depth, 80-115 m/s, µm	Average Reaction Depth, 150-200 m/s, µm	Impingement Depth, 200-235 m/s, µm
Sc	44 ± 2 *	44 ± 2 *	241 ± 10
Nd	155 ± 5 ⁺	142 ± 7 ⁺	-
Er	50 ± 3	16 ± 3	42 ± 7
Yb	51 ± 2	22 ± 3	37 ± 6
Lu	32 ± 2	22 ± 3	90 ± 4

(Sc,Y,Yb)	45 ± 2	38 ± 3	100 ± 23
(Er,Yb,Lu)	41 ± 1	26 ± 5	53 ± 12
(Y,Er,Yb,Lu)	39 ± 2	18 ± 3	57 ± 8
(Sc,Nd,Er,Yb,Lu)	47 ± 3	29 ± 8	33 ± 16

Acknowledgements

This work was supported by the National Science Foundation DMREF: Collaborative Research: GOALI: Accelerating Discovery of High Entropy Silicates for Extreme Environments (Dr. Elizabeth Opila, Dr. Patrick Hopkins, Dr. Jon Ihlefeld, Dr. Cormac Toher), Award #1921973, the Virginia Space Grant Consortium 2020-2021 graduate fellowship, and the Nanoscale Materials Characterization Facility at the University of Virginia.

References

1. Steibel J, Ren Z, Singh G, Misra A, Lee KN, van Roode M. Ceramic matrix composites taking flight at GE aviation. *American Ceramic Society Bulletin*. 2019;(98):30–33.
2. Olesinski RW, Abbaschian GJ. The C−Si (Carbon-Silicon) System. *Bulletin of Alloy Phase Diagrams*. 1984;(5):486–489.
3. Opila EJ, Smialek JL, Robinson RC, Fox DS, Jacobson NS. SiC Recession Caused by SiO_2 Scale Volatility under Combustion Conditions: II, Thermodynamics and Gaseous-Diffusion Model. *Journal of the American Ceramic Society*. 1999;82(7):1826–1834.
4. Felsche J. Rare Earth Silicates with the Apatite Structure. *Journal of Solid State Chemistry*. 1972;5:266–275. https://doi.org/10.1016/0022-4596(72)90039-4
5. Hoai Le T, Tang K, Arnout S, Malfliet A, Blanpain B, Guo M. Thermodynamic assessment of the Nd_2O_3-CaO-SiO_2 ternary system. *Calphad*. 2016;55:157–164. https://doi.org/10.1016/j.calphad.2016.08.006
6. Toropov NA, Galakhov FYa, Konovalova SF. *Bull Acad Sci USSR, Div Chem Sci*. 1961;8:1271–1277.
7. Turcer LR, Padture NP. Towards multifunctional thermal environmental barrier coatings (TEBCs) based on rare-earth pyrosilicate solid-solution ceramics. *Scripta Materialia*. 2018;154:111–117. https://doi.org/10.1016/j.scriptamat.2018.05.032
8. Opila EJ, Hann RE. Paralinear Oxidation of CVD SiC in Water Vapor. *Journal of the American Ceramic Society*. 1997;80(1):197–205. https://doi.org/10.1111/j.1151-2916.1997.tb02810.x
9. Ferber MK, Lin HT. Environmental Characterization of Monolithic Ceramics for Gas Turbine Applications. *Key Eng Mat*. 2005;287:367–380. https://doi.org/10.4028/www.scientific.net/KEM.287.367
10. Gild J, Braun J, Kaufmann K, *et al.* A High-entropy Silicide: $(Mo_{0.2}Nb_{0.2}Ta_{0.2}Ti_{0.2}W_{0.2})Si_2$. *Journal of Materiomics*. 2019;5(3):337–343. https://doi.org/10.1016/j.jmat.2019.03.002
11. Miracle DB, Senkov ON. A critical review of high entropy alloys and related concepts. *Acta Materialia*. 2017;122:448–511.
12. DeHoff R. Thermodynamics in Materials Science, Second Edition. CRC Press; 2006
13. Ushakov SV, Hayun S, Gong W, Navrotsky A. Thermal Analysis of High

Entropy Rare Earth Oxides. *Materials*. 2020;13(14):3141. https://doi.org/10.3390/ma13143141

14. Fernández-Carrión AJ, Alba MD, Escudero A, Becerro AI. Solid Solubility of $Yb_2Si_2O_7$ in β-, γ- and δ-$Y_2Si_2O_7$. *Journal of Solid State Chemistry*. 2011;184(7):1882–1889. https://doi.org/10.1016/j.jssc.2011.05.034
15. Dong Y, Ren K, Lu Y, Wang Q, Liu J, Wang Y. High-entropy environmental barrier coating for the ceramic matrix composites. *Journal of the European Ceramic Society*. 2019;39(7):2574–2579. https://doi.org/10.1016/j.jeurceramsoc.2019.02.022
16. Sun L, Luo Y, Tian Z, *et al.* High temperature corrosion of $(Er_{0.25}Tm_{0.25}Yb_{0.25}Lu_{0.25})_2Si_2O_7$ environmental barrier coating material subjected to water vapor and molten calcium–magnesium–aluminosilicate (CMAS). *Corrosion Science*. 2020;175:108881. https://doi.org/10.1016/j.corsci.2020.108881
17. Ridley M, Opila E. Thermochemical stability and microstructural evolution of $Yb_2Si_2O_7$ in high-velocity high-temperature water vapor. *Journal of the European Ceramic Society*. 2020;41(5):3141–3149. https://doi.org/10.1016/j.jeurceramsoc.2020.05.071
18. Braun JL, Olson DH, Gaskins JT, Hopkins PE. A steady-state thermoreflectance method to measure thermal conductivity. *Review of Scientific Instruments*. 2019;90(2):024905. https://doi.org/10.1063/1.5056182
19. Ridley MJ, Gaskins J, Hopkins P, Opila EJ. Tailoring Thermal Properties of Multi-component Rare Earth Monosilicates. *Acta Materialia*. 2020;195:698–707. https://doi.org/10.1016/j.actamat.2020.06.012
20. Tian Z, Zheng L, Li Z, Li J, Wang J. Exploration of the low thermal conductivities of γ-$Y_2Si_2O_7$, β-$Y_2Si_2O_7$, β-$Yb_2Si_2O_7$, and β-$Lu_2Si_2O_7$ as novel environmental barrier coating candidates. *Journal of the European Ceramic Society*. 2016;36(11):2813–2823. https://doi.org/10.1016/j.jeurceramsoc.2016.04.022
21. Tian Z, Zheng L, Wang J, Wan P, Li J, Wang J. Theoretical and experimental determination of the major thermo-mechanical properties of RE_2SiO_5 (RE=Tb, Dy, Ho, Er, Tm, Yb, Lu, and Y) for environmental and thermal barrier coating applications. *Journal of the European Ceramic Society*. 2016;36(1):189–202. https://doi.org/10.1016/j.jeurceramsoc.2015.09.013
22. Abeles B. Lattice Thermal Conductivity of Disordered Semiconductor Alloys at High Temperatures. *Phys Rev*. 1963;131(5):1906–1911. https://doi.org/10.1103/PhysRev.131.1906
23. Giri A, Braun J, Rost C, Hopkins P. On the minimum limit to thermal conductivity of multi-atom component crystalline solid solutions based on impurity mass scattering. *Scripta Materialia*. 2017;(138):134–138. https://doi.org/10.1016/j.scriptamat.2017.05.045